Atomic Force Microscopy of Cellulose Membranes Prepared from the *N*-Methylmorpholine-*N*-oxide/Water Solvent System

Yaopeng Zhang, Huili Shao, Xuechao Hu

State Key Laboratory for Modification of Chemical Fibers and Polymer Materials, Dong Hua University, Shanghai 200051, China

Received 13 August 2001; accepted 12 March 2002

ABSTRACT: Cellulose membranes were obtained by solutions of cellulose being cast into a mixture of *N*-methylmorpholine-*N*-oxide (NMMO) and water under different processing conditions. Atomic force microscopy (AFM) was used to investigate the surface structures of the membranes. The AFM method provided information on both the size and shape of the pores on the surface, as well as the roughness of the skin, through a computerized analysis of AFM micrographs. The results obtained showed that the surface morphologies were intrinsically associated with the permeation properties. For the cellulose membranes, increasing the NMMO concentration and the temperature of the coagulation bath led to higher fluxes and lower bovine serum albumin rejection. These were always correlated with higher values of the roughness parameters and larger pore sizes of the membrane surfaces. When the cellulose concentration of the casting solution was 11 wt %, the membrane showed a nodular structure with interconnected cavity channels between the agglomerated nodules. © 2002 Wiley Periodicals, Inc. J Appl Polym Sci 86: 3389–3395, 2002

Key words: membranes; atomic force microscopy (AFM)

INTRODUCTION

Since its invention in 1986, atomic force microscopy (AFM) has evolved as a valuable imaging technique, with a resolution in the micrometer to subnanometer range.[1] The AFM imaging of membrane structures has advantages over scanning electron microscopy and transmission electron microscopy because the resolution is higher, the sample preparation is minimal, and no electron-beam damage can occur. Moreover, this powerful imaging device allows the topographical study of membrane surfaces both in air and in process-relevant aqueous environments without special sample preparation.[2] The technique has, therefore, been applied to the study of membranes, including microfiltration and ultrafiltration (UF) membranes,[3–5] nanofiltration membranes,[6,7] and gas-separation membranes,[8,9] giving useful information about surface morphology, surface pore size distributions, surface porosity, and surface roughness.

An atomic force microscope may be used in a number of different modes.[10] The most widely used is the contact mode, in which the tip responds to very short range repulsive (Born) forces. A second mode of operation is the noncontact mode, in which the tip responds to attractive van der Waals interactions with the sample. These have been the most widely used modes, and virtually all AFM membrane studies have been carried out in these modes.

In this work, contact-mode atomic force microscopy (CM AFM) was used to comply with the main objective of differentiating the surface morphologies of membranes in the UF range. The aim of this AFM characterization was to determine the correlation of the membrane surface morphologies and the membrane permeation properties.

EXPERIMENTAL

Materials

A cellulose sample was purchased from Shanghai Fengxian Pulp Co. (Shanghai, China). Fifty percent *N*-methylmorpholine-*N*-oxide (NMMO), obtained from BASF (Ludwigshafen, Germany), was used as the solvent after being concentrated to 87 wt % (NMMO/H_2O = 87/13, expressed with NMMO), in addition to 0.5 wt % *n*-propylgallate (supplied by Shanghai Reagents Co., Shanghai, China), which was used as an antioxidant to avoid oxidation and degradation during the cellulose dissolving process.

Membrane preparation

Cellulose pulp was dried in a vacuum oven at 60°C for 12 h for the removal of absorbed water before use and was dissolved in NMMO and an antioxidant.[11] The solution was cast onto a glass plate (250 μm thick) at room temperature. The cellulose solution on the glass

Correspondence to: X. Hu (xchu@dhu.edu.cn).

Journal of Applied Polymer Science, Vol. 86, 3389–3395 (2002)

TABLE I
Casting Solutions and the Conditions of Coagulation for Membrane Formation

Membrane	Casting solution concentration (wt %)	Temperature of coagulation bath (°C)	NMMO concentration of coagulation bath (vol %)
T-20		20	
T-35	7	35	0
T-45		45	
T-55		55	
N-7.5			7.5
N-15	7	25	15
N-30			30
C-9	9		
C-11	11	25	0

plate was immediately immersed in a coagulation bath of an aqueous NMMO solution for several minutes. After coagulation, the membranes were transferred to a water bath for 24 h for the complete removal of the excess solvent. Then, the samples were soaked in a 30 vol % glycerol solution for 10 min before being air-dried for at least 24 h at room temperature. The membranes were prepared under different processing conditions, including the temperature and NMMO concentration of the coagulation bath and the cellulose concentration of the casting solution. The codes of the samples and detailed preparation conditions are listed in Table I.

Permeation experiments

The obtained membrane sheet was cut into circular membrane species 43 mm in diameter before use. All filtration experiments were carried out at 25°C under 2 kPa of applied pressure.

The permeation experiments were carried out with deionized water to determine the membrane pure water flux (J) and with a reference solution of bovine serum albumin (BSA; molecular weight = 67,000; Boehringer Mannheim Biochemicals, Mannheim, Germany) to determine the rejection to this protein (R).

J is calculated as follows:

$$J = \frac{V}{tS} \tag{1}$$

where V is the total volume of the water permeated during the experiment, t is the operation time, and S is the membrane area.[12] R is defined as

$$R = \left(1 - \frac{C_p}{C_f}\right) \times 100\% \tag{2}$$

where C_p and C_f are the concentrations of BSA in the permeate and in the feed, respectively, obtained with a model 7520 spectrophotometer (Shanghai Analytical Instrument Factory, Shanghai, China) at a wavelength of 280 nm.[13,14]

AFM images

The atomic force microscope used to image the membrane surfaces was a multimode scanning probe microscope with a Nanoscope IIIa controller, supplied by Digital Instruments (Santa Barbara, CA). The membrane surface was scanned in the contact mode.

Small pieces were cut from each membrane, glued onto metal disks, and attached to a magnetic sample holder located on top of the scanner tube. All the CM AFM images were undertaken at 25°C.

The AFM software allows image representation in the top view and in perspective and allows the quantitative determination of the diameter of pores by the use of the images in conjunction with digitally stored line profiles.[15] The simultaneous use of the images and profiles greatly facilitates the identification of the entrance of individual pores (however, the diameter deep in the membrane may not be determined directly by surface AFM because of the convolution between the tip shape and the pore). Pore diameters were determined in this way for a minimum of 40 pores on each membrane.

Moreover, the AFM image analysis software allows a roughness analysis for both selected areas and membranes. Differences in the membrane surface morphology can be expressed in terms of various roughness parameters:[16]

1. The difference between the highest and the lowest points within the given area (z).
2. The standard deviation of the z values within the given area (R_q). This parameter is calculated as follows:

$$R_q = \sqrt{\frac{\sum (z_i - z_{\text{avg}})^2}{N_p}}$$

TABLE II
Permeation Properties and Surface Analysis of Membranes

	Permeation properties		Pore size statistical analysis				Roughness analysis		
Membrane	J (mL/cm^2 h)	R (%)	μ (nm)	σ (nm)	Minimum size (nm)	Maximum size (nm)	z (nm)	R_q (nm)	R_a (nm)
T-20	0.70	41.5	99.87	25.08	54.69	171.9	19.46	3.016	2.422
T-35	1.08	14.3	106.4	29.82	54.69	179.7	24.10	2.856	2.224
T-45	1.11	<5	145.4	35.92	93.75	281.3	24.15	2.899	2.256
T-55	4.7	<5	175.2	46.40	93.75	328.1	66.59	9.611	7.702
N-7.5	0.64	<5	170.3	49.61	93.75	312.5	15.62	2.027	1.600
N-15	0.89	<5	177.0	48.69	93.75	312.5	15.08	2.264	1.807
N-30	1.27	<5	227.0	65.56	125.0	406.3	27.44	2.545	1.908
C-9	2.68	72.4	159.6	32.20	101.6	234.4	45.40	6.667	5.253
C-11	1.08	81.6	98.70	26.59	54.09	171.9	74.67	5.592	4.174

where z_i is the current z value, z_{avg} is the average of the z values within the given area, and N_p is the number of points within the given area.

3. The mean roughness (R_a). This parameter represents the mean value of the surface relative to the center plane, the plane for which the volumes enclosed by the image above and below this plane are equal. It is calculated as follows:

$$R_a = \frac{1}{L_x L_y} \int_0^{L_x} \int_0^{L_y} |f(x,y)| dx\, dy$$

where $f(x,y)$ is the surface relative to the center plane and L_x and L_y are the dimensions of the surface in the x and y directions, respectively.

All the surface roughness parameters were calculated from the AFM images with an AFM software program.

RESULTS AND DISCUSSION

The data given in Table II report J and R of the cellulose membranes prepared under various conditions. The corresponding pore size statistics and roughness parameters, which were obtained from the AFM images presented later in Figures 1, 3, and 5 with the use of an appropriate software program, are also shown in Table II. All images were flattened in the same way, and so the roughness values are relative and not absolute values.

Effect of the temperature of the coagulation bath

Figure 1 shows three-dimensional (3D) CM AFM images for the surfaces of the T-20, T-35, T-45, and T-55 membranes over a selected area of 2 μm $\times$ 2 μm. The pores, which are well-defined dark areas on the images, are clearly visible. The effect of the temperature of the coagulation bath (pure water) is clearly illustrated by a comparison of the four images in Figure 1. In the active layer of the membranes prepared from the coagulation bath with a higher temperature, the average size of the darker depression areas observed in the AFM 3D images is larger than that for the membranes prepared from the coagulation bath with a lower temperature. Figure 2 shows the pore size distribution for these pores, with its statistical analysis given in Table II. When the temperature of the pure water bath increases from 20 to 55°C, the mean pore size (μ) of the membranes increases from 99.9 to 175.2 nm. Also, the pore size distribution, which can be represented by the standard deviation (σ), becomes wider when the temperature of the coagulation bath is higher. The larger values of μ and σ are associated with the increase in J and the decrease in R with the increasing temperature. The results show that the membranes have almost no rejection (<5%) to BSA when μ is larger than 145 nm. The difference in the surface morphologies is also illustrated by the values of the statistical parameters R_a and z, which are much higher for T-55.

When a casting solution is immersed in the coagulation bath, the casting solution of the surface splits into a polymer-poor phase and a polymer-rich phase.[17] After solidification, the polymer-poor phase becomes pores, and the polymer-rich phase develops into a polymer matrix.[18] It is believed that the solidification of a cellulose solution is more rapid when the temperature of the coagulation bath is higher. That is due to the higher diffusion rates of NMMO and water. Accordingly, for a higher temperature of the coagulation bath, demixing occurs throughout the polymer solution instantly during the rapid solidification process. Therefore, the polymer is solidified before the merging of the polymer-rich phase, and larger pores are formed in comparison with those of the membranes prepared from the coagulation bath with a lower temperature.

Effect of the NMMO concentration of the coagulation bath

Figure 3 shows a set of images of the N-7.5, N-15, and N-30 membranes covering areas of 2 μm $\times$ 2 μm. Pore

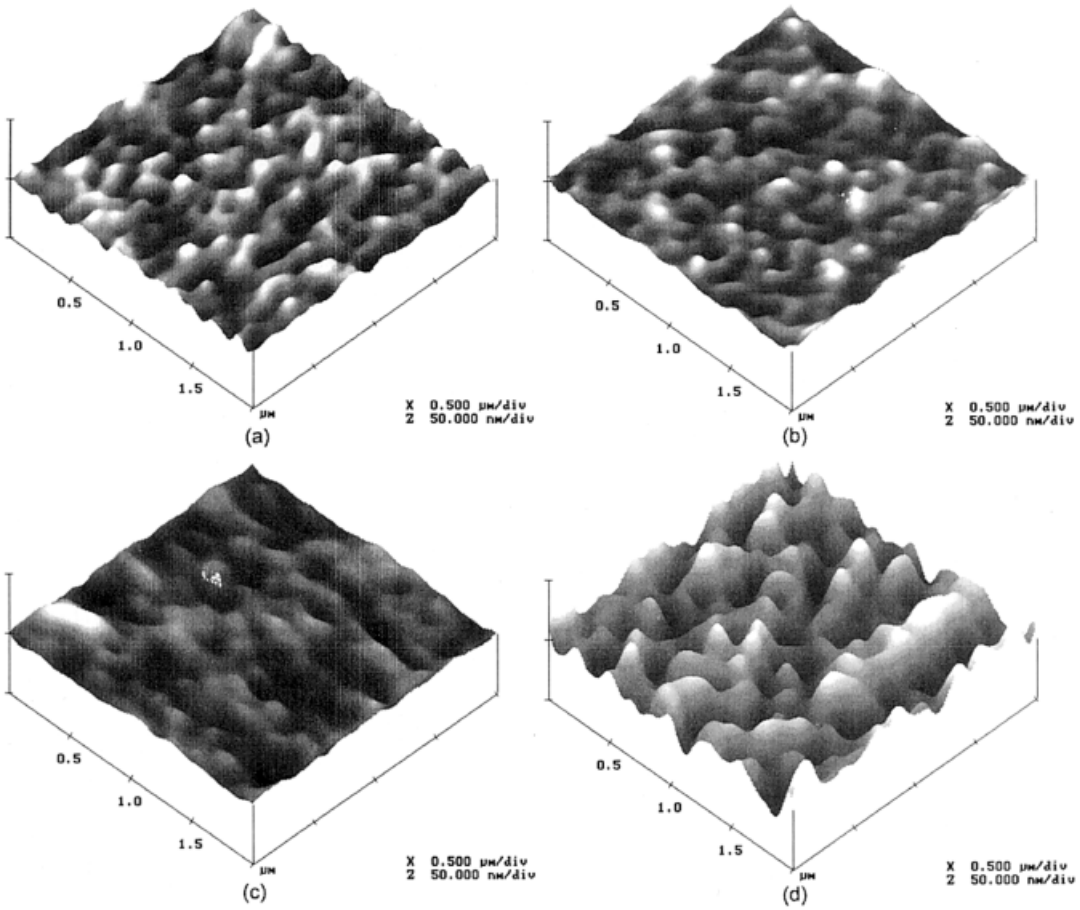

Figure 1 AFM images of cellulose membranes: (a) T-20, (b) T-35, (c) T-45, and (d) T-55.

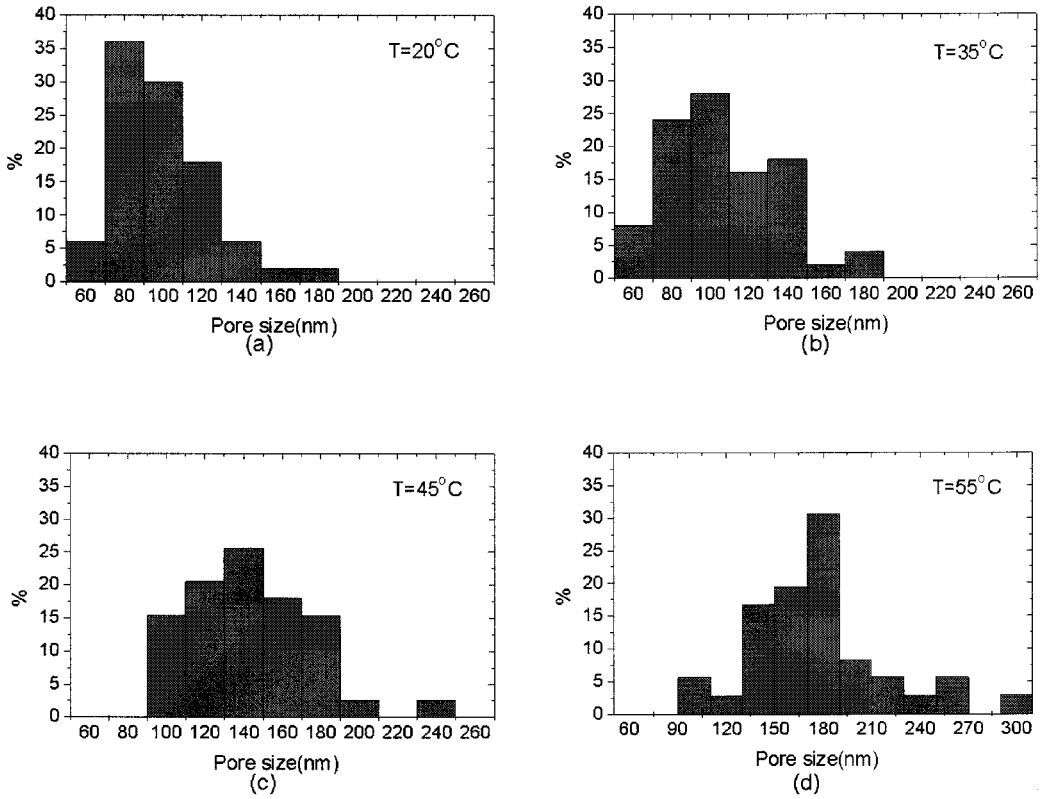

Figure 2 Pore size distributions of cellulose membranes obtained from AFM images: (a) T-20, (b) T-35, (c) T-45, and (d) T-55.

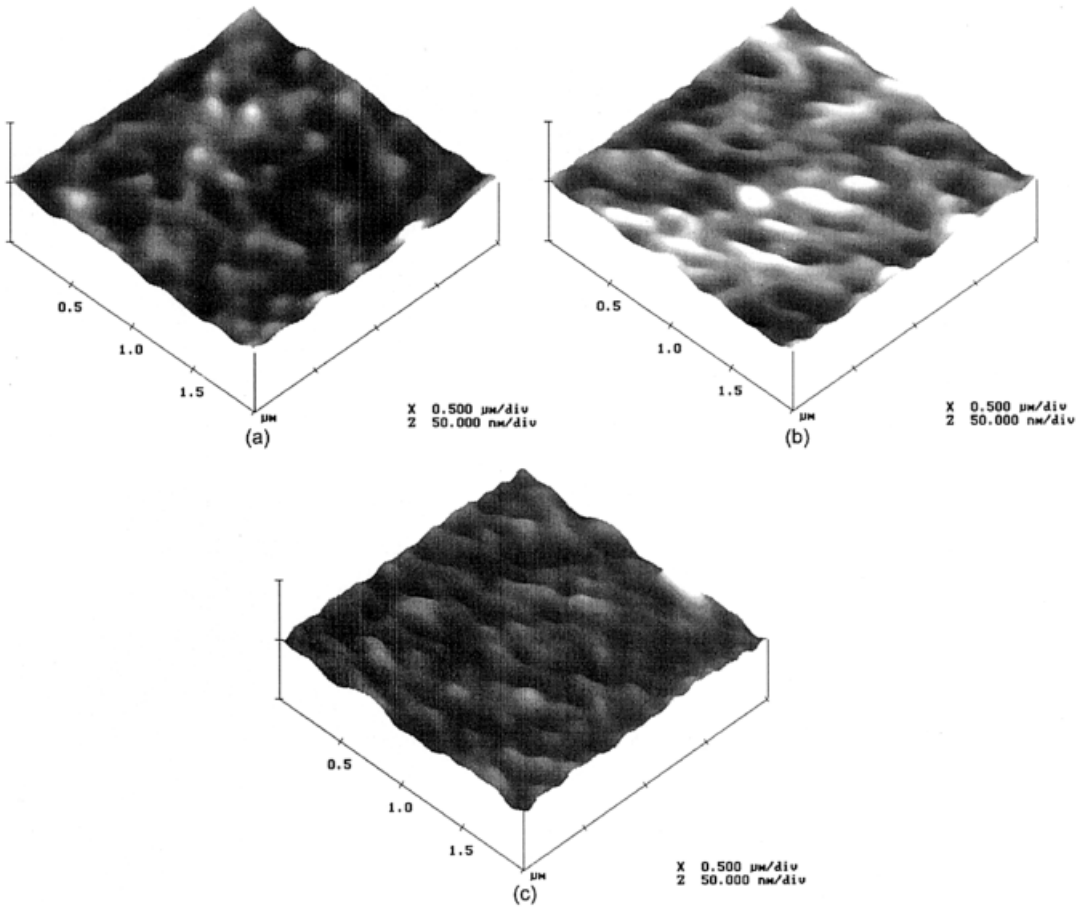

Figure 3 AFM images of cellulose membranes: (a) N-7.5, (b) N-15, and (c) N-30.

size distributions based on these three images are shown in Figure 4, with the statistical information summarized in Table II. The temperatures of the coagulation bath in this series were kept at 25°C. Again, the pore size increases and the pore size distribution tends to be wider with the increasing NMMO concentration of the coagulation bath. However, the variations of the pore sizes of these three membranes are much less evident than those of the membranes coagulated from a pure water bath with a different temperature. This implies that the effect of the coagulation bath temperature on the membrane morphology is greater than that of the NMMO concentration, although both increase μ of the membranes. By comparing the roughness analysis results of these three samples, we have also found that both R_a and z tend to be higher for a higher NMMO concentration. As a result of larger pore sizes and higher values of the roughness parameters of the membranes, an increase of J from 0.64 h to 1.27 mL/cm^2 h can be observed. These results are shown in Table II. In addition, the rejection to BSA is very low because of the excessively large pore size (>145 nm) of the membranes.

There is a general consensus among researchers that, in the case of immersion precipitation, liquid–liquid demixing processes are largely responsible for the membrane morphology.[19–21] Nevertheless, the attribution of specific structures in the membrane to phase-separation processes is even more complicated for ternary systems than for binary systems. The reason for these difficulties is that the diffusion processes change the initial composition of the film directly after immersion. Also, the composition is not the same throughout the solution. The mechanism of formation of the top layer can differ from the mechanism of formation for the layer close to the support. The delay time for demixing is an important parameter in determining the membrane morphologies. It is approximately 1 s or less for rapid demixing conditions. For delayed demixing, the precipitation time is seconds to minutes.

The delay time will increase when a solvent is added to the coagulation bath. Therefore, the growth of the polymer-poor droplets through the interface can progress for some period before the solidification of the polymer-rich phase because the solidification rate would be slow on account of the low diffusion rates of the solvent and water. The fixation of the membrane structure will also be delayed because of the depression of the glass transition of the polymer by the solvent. Coarsening can continue for a longer time period, and the pores will become larger. Wijmans et al.[22] demonstrated that membranes with a porous top

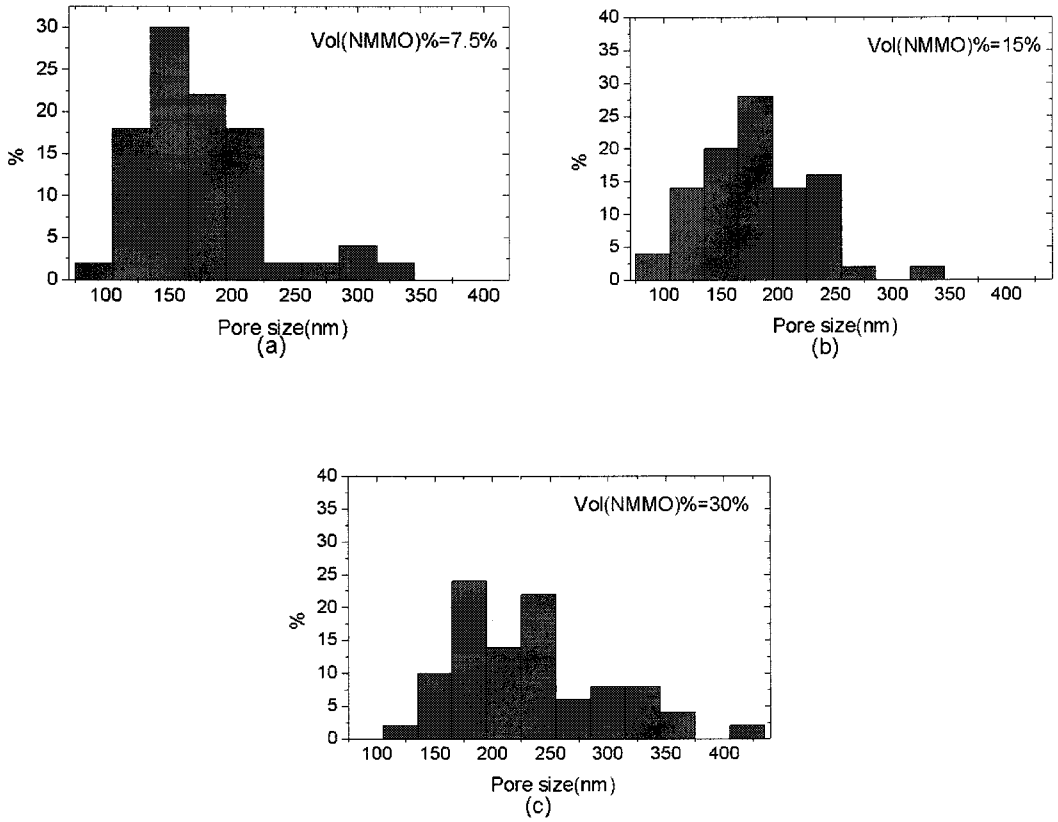

Figure 4 Pore size distributions of cellulose membranes obtained from AFM images: (a) N-7.5, (b) N-15, and (c) N-30.

layer can be obtained when the concentration of the solvent in the coagulation bath exceeds a certain minimum value. That is the reason that in this case the pore size of the resulting membrane is larger when the NMMO concentration of the coagulation bath increases.

Effect of the cellulose concentration of the casting solution

Figure 5 shows images of C-9 and C-11 membranes covering areas of 2 μm $\times$ 2 μm. One can easily identify the differences in the surface structures of the two membranes in Figure 5. Figure 5(a) shows a typical pore structure of a membrane in which large pores exist throughout the whole membrane surface. However, a nodular structure with interconnected cavity channels between the agglomerated nodules exists for C-11 [Fig. 5(b)]. It is believed that the cellulose concentration affects the chain entanglement. For a higher cellulose concentration (C-11), cellulose in the polymer-rich phase has less ability to deform and merge and yields nodules because of the increase in chain entanglement and the consequent interruption of free chain mobility during coagulation. At the mean time

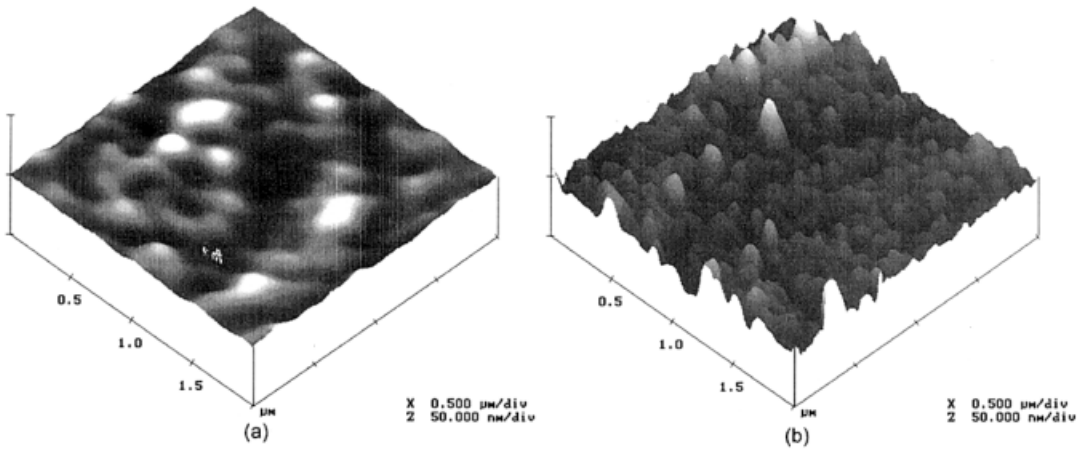

Figure 5 AFM images of cellulose membranes: (a) C-9 and (b) C-11.

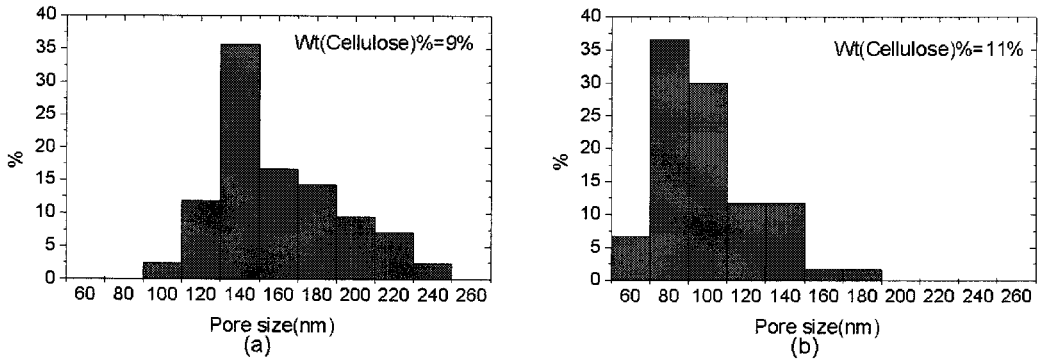

Figure 6 Pore size distributions of cellulose membranes obtained from AFM images: (a) C-9 and (b) C-11.

of solidification, the polymer-poor phase becomes interstitial cavities on the top layer of the membrane. The C-9 membrane prepared from a casting solution with a 9 wt % cellulose concentration shows a porous structure. The morphology is believed to be the result of lower polymer chain entanglement and larger free chain mobility.[23]

From an analysis of the interstitial cavities of Figure 5(a) and the pores of Figure 5(b), the pore size distributions are shown in Figure 6. The statistical information is summarized in Table II. As expected, a higher cellulose concentration of the casting solution results in a smaller pore size because of the higher polymer net density. It can also be seen in Table II that the C-11 membrane prepared from a casting solution with an 11 wt % cellulose concentration displays lower flux and higher rejection in comparison with C-9. In this case, a higher value of R_a is also obtained and is associated with the results for J and R.

CONCLUSIONS

Cellulose membranes have been prepared under different processing conditions and have shown different UF permeation properties, which can be explained very well with AFM investigations. AFM is an effective method for investigating the surface structures of membranes. This work has shown that it is possible to image the surface of cellulose membranes, and image analysis can provide detailed information on the surface roughness and pore structure and allows the quantitative determination of the pore size distribution.

Increasing the temperature and NMMO concentration of the coagulation bath leads to larger pore sizes, wider pore size distributions, and higher values of the roughness parameters. As a result, the membranes display higher fluxes and lower rejections of BSA. However, the effect of the temperature of the coagulation bath on the membrane morphology is greater than the effect of the NMMO concentration in the coagulation bath.

When the cellulose concentration of the casting solution is 11 wt %, the membrane surface shows a different nodular structure with interconnected cavity channels between the agglomerated nodules. A higher cellulose concentration results in a membrane with a smaller pore size, lower flux, and higher rejection.

References

1. Bowen, W. R.; Hilal, N.; Lovitt, R. W.; Williams, P. M.; Wright, C. J. In Surface Chemistry and Electrochemistry of Membrane Surfaces; Sorensen, T. S., Ed.; Surfactant Science Series; Marcel Dekker: New York, 1999; Chapter 1, p 2.
2. Bowen, W. R.; Doneva, T. A. J Membr Sci 2000, 171, 141.
3. Bessieres, A.; Meireles, M.; Cotatger, R.; Beauvillain, J.; Sanchez, V. J Membr Sci 1996, 109, 271.
4. Bowen, W. R.; Hilal, N.; Lovitt, R. W.; Williams, P. M. J Membr Sci 1996, 110, 233.
5. Bowen, W. R.; Mohammad, A. W.; Hilal, N. J Membr Sci 1997, 126, 91.
6. Bowen, W. R.; Hilal, N.; Lovitt, R. W.; Williams, P. M. J Membr Sci 1998, 139, 269.
7. Singh, S.; Khulbe, K. C.; Matsuura, T.; Ramamurthy, R. P. J Membr Sci 1998, 142, 111.
8. Khulbe, K. C.; Kruczek, B.; Chowdhury, G.; Gagne, S.; Matsuura, T. J Appl Polym Sci 1996, 59, 1151.
9. Khulbe, K. C.; Kruczek, B.; Chowdhury, G.; Gagne, S.; Matsuura, T.; Verma, S. P. J Membr Sci 1996, 111, 57.
10. Bowen, W. R.; Hilal, N.; Lovitt, R. W.; Sharif, A. O.; Williams, P. M. J Membr Sci 1997, 126, 77.
11. Zhang, Y.; Shao, H.; Wu, C.; Hu, X. Macromol Biosci 2001, 1, 142.
12. Yang, G.; Zhang, L. J Membr Sci 1996, 114, 152.
13. Jian, X.; Dai, Y.; He, G.; Chen, G. J Membr Sci 1999, 161, 187.
14. Wang, X.; Spencer, H. G. J Appl Polym Sci 1998, 67, 514.
15. Calvo, J. I.; Pradanos, P.; Hernandez, A.; Bowen, W. R.; Hilal, N.; Lovitt, R. W.; Williams, P. M. J Membr Sci 1997, 128, 10.
16. Stamatialis, D. F.; Dias, C. R.; de Pinho, M. N. J Membr Sci 1999, 160, 237.
17. Cheng, L. P.; Soh, Y. S.; Dwan, A.; Gryte, C. C. J Polym Sci Part B: Polym Phys 1994, 32, 1413.
18. Pereira, S.; Inoue, T. J Membr Sci 1996, 111, 93.
19. van de Witte, P.; Dihkstra, P. J.; van den Berg, J. W. A.; Feijen, J. J Membr Sci 1996, 117, 19.
20. Radovanovic, P.; Thiel, S. W.; Hwang, S.-T. J Membr Sci 1992, 65, 231.
21. Reuvers, A. J.; Smolders, C. A. J Membr Sci 1987, 34, 67.
22. Wijmans, J. G.; Baaij, J. P. B.; Smolders, C. A. J Membr Sci 1983, 14, 263.
23. Bang, Y. H.; Lee, S.; Park, J. B.; Cho, H. H. J Appl Polym Sci 1999, 163, 2689.